Sensitivity of simulated wintertime Arctic atmosphere to vertical resolution in the ARPEGE/IFS model

Øyvind Byrkjedal*,

Geophysical Institute, University of Bergen
Bjerknes Centre for Climate Research

Igor Esau

Nansen Environmental and Remote Sensing Center
Bjerknes Centre for Climate Research

Nils Gunnar Kvamstø

Geophysical Institute, University of Bergen
Bjerknes Centre for Climate Research

_____

* Corresponding author:
    Bjerknes Centre for Climate Research, University of Bergen
    Allegt 55, 5007 Bergen, Norway
    E-mail: Oyvind.Byrkjedal@bjerknes.uib.no
    Tel: + 47-55582594 Fax: + 47-55589883

Abstract

The current state of the art general circulation models, including several of those used by the IPCC, show considerable disagreement in simulating present day high latitude climate. This is of major concern and reduces the confidence in future model projections of high latitude climate.

We here employ ideal vertical profiles of temperature and wind from turbulence resolving simulations to perform *a priori* studies of the first order eddy-viscosity closure scheme employed in the ARPEGE/IFS model. This reveals that the coarse vertical resolution (31 layers) of the model cannot be expected to realistically resolve the Arctic stable boundary layer. The curvature of the Arctic inversion and thus also the vertical turbulent exchange processes cannot be reproduced by the coarse vertical mesh employed. Correct representation of boundary layer turbulent exchange processes is a critical factor in climate simulations.

To investigate how turbulent vertical exchange processes in the Arctic boundary layer are represented by the model parameterization a simulation with high vertical resolution (90 layers) in the lower part of the atmosphere is performed. Results from the model simulations are validated against data from the ERA-40 reanalysis and from in situ data from the SHEBA project. The dependence of the surface air temperature on surface winds, surface energy fluxes, inversion stability and boundary layer height is investigated. The coarse resolution run reveals considerable biases in these parameters, and in their physical relations to surface air temperature. In the simulation with fine vertical resolution these biases are clearly reduced. The physical relation between governing parameters for the vertical turbulent exchange processes becomes more realistic.

The coarse resolution run shows considerable biases in representing the Arctic inversion. By improving the vertical resolution in the lower part of the atmosphere we achieve a realistic simulation of the Arctic inversion. A correct representation of the inversion is important in order to achieve a realistic representation of radiation and cloud processes in the Arctic.

1. Introduction

Vertical resolution of climate models has not been a focal issue for sensitivity studies. This is surprising since the non-linear vertical profiles of all model variables usually exhibit strong curvature in the first 1 km above the surface. Sufficient resolution of this layer is also important both for climate and weather prediction simulations. The lowest atmospheric layer comprises the densest clouds and intense turbulent activity. Tompkins and Emanuel (2000) demonstrated that equilibrium climate simulations are not possible with a resolution coarser than 25 hPa (about 200 m) within a planetary boundary layer as the vertical temperature and moisture profiles do not converge toward radiative-convective equilibrium. The majority of models (Tao et al. 1996) have only 7 to 30 layers in the total vertical column with only 3 to 7 layers placed within the first 1000m of the atmosphere. The models generally show considerable improvement with increasing vertical resolution (e.g. Hogan and Brody 1993; Slingo et al. 2004). However, it has been found that merely improving the vertical resolution to a few hundred meters does not affect the simulation results significantly (Boville 1991). The earlier studies were able to compare only very coarse vertical resolution models. Recent dynamical downscaling studies (e.g. Lane et al. 2000) suggest that considerable refinement (to 60 vertical levels or more) of the vertical resolution is needed to achieve visible improvement in simulations. A recent study (Roeckner et al. 2006), using the ECHAM5 model, concluded that increasing the horizontal resolution while keeping a fixed coarse vertical resolution (L19, i.e. 19 vertical levels), does not lead to convergence toward a more realistic climate state. However, by increasing also the vertical resolution (L31) simulations with high horizontal resolution do converge monotonically toward the more realistic climate state. The L31 runs performed better at all horizontal resolutions for the boreal winter. Compared to the ERA-40 reanalysis (Uppala et al. 2005), the coarser ECHAM5 model climate is too cold north of 60°N throughout the entire atmospheric column. It shares this feature with the majority of regional models in the ARCMIP – Arctic model intercomparison project (Tjernstrom et al. 2004; Rinke et al. 2006). Refinement of the vertical resolution leads to a warming of the Arctic atmosphere in those models.

The majority of the IPCC models, including the atmospheric component of the Bergen Climate Model – ARPEGE/IFS (Deque et al. 1994) – have a warm bias in the Arctic wintertime climate (Tao et al. 1996). Bossuet et al. (1998) studied differences in the ARPEGE climate for 41L and 31L runs but did not find any significant changes in the polar

troposphere. As we will show in this study, these results are to be expected. Their 41L run retained quite coarse vertical resolution in the boundary layer with the first levels at 43 m, 140 m, and 281 m. In situ intercomparison studies with single-column models (Lane et al. 2000) suggest that 60 or more vertical levels are required in order to achieve convergence of radiation and cloud schemes in the model.

The sensitivity studies mentioned do not resolve the main features of the Arctic wintertime temperature profiles in the lower troposphere. Adequate simulations of those profiles are important for a correct description of the turbulent mixing. The development of turbulent mixing in the Arctic is inhibited by a number of factors: Negative radiation balance at the surface, strong air subsidence in the mid-troposphere, and temperature inversions formed by advective, radiative and subsidence processes. Weak turbulent mixing is unable to compensate radiative surface cooling by increasing the downward sensible flux from the warm atmospheric inversion layer (Overland and Guest 1991). Persistent surface cooling results in the gradual formation of very low wintertime temperatures in the lower troposphere becoming the main feature of the Arctic climate.

Models with a warm bias obviously have difficulties reproducing the low temperatures of the sub-inversion layer. The summary report on Arctic climate and modelling (ACIA 2004) disclosed a serious discrepancy between observed and modelled geographical patterns of the Arctic climate evolution over the last 50 years. An in situ study with the ECMWF model (Beesley et al. 2000) showed that the model systematically misses extremes in the surface air temperature (SAT) in comparison with SHEBA (Uttal et al. 2002) data. The model tends not to produce low temperatures in response to weak mechanical forcing, but raises the temperature rather rapidly in response to warm air advection. This tends to cause a warm bias in the SAT, with the largest warm bias located in areas with the climatologically lowest surface temperatures (Kiehl and Gent 2004 for CCSM-2). Recent intercomparisons by Cuxart et al. (2006) traced this problem to excessive turbulent fluxes in 25 turbulence schemes from research and climate models. Such schemes use constraints on the minimum possible flux (Louis 1979; Beljaars and Viterbo 1999) in order to prevent atmosphere-surface decoupling and consequent model instabilities.

Randall et al. (1998) performed a survey of Arctic climate modelling, and recognized gaps in our understanding of the interactions between cloud, radiation, ice, and boundary layer

processes. These gaps are large enough to question the models' reliability for Arctic climate prediction. At present, mainstream studies try to improve model performance in cold climates through development of even more sophisticated vertical diffusivity schemes. For instance, the ARPEGE/IFS model now incorporates three different schemes providing independent and quite different vertical fluxes for different purposes. Intercomparison by Cuxart et al. (2006) has shown that the more sophisticated schemes do not necessarily improve performance compared to simpler schemes. Dethloff et al. (2001) compared the performance of single-column models (ECHAM3 and HIRLAM) employing analytical turbulence diffusion schemes of the resistance-law type (Zilitinkevich and Esau 2005) with more traditional, eddy-viscosity type schemes employed in the same models. The analytical schemes exhibited a considerable improvement in performance. One hypothesis, which will be tested in this study, is that the analytical schemes prescribe the correct vertical flux profile in the cases where the eddy-viscosity schemes cannot produce realistic fluxes due to the lack of vertical resolution. A popular, but undesirable, solution is to tune those schemes towards ideal data sets (e.g. for ARPEGE model see Bazile et al. 2005). To our knowledge however, those tuning exercises have been limited to certain in situ cases and thus suffer from a lack of generality.

We will here investigate the effect of vertical resolution refinement on the model climate. Using guidelines from turbulence-resolving models (e.g. Beare et al. 2006), we determine a minimum vertical resolution and adequate level spacing in the model. We will compare simulations with 31 (31L) and 90 (90L) vertical levels. Section 2 describes the general circulation model ARPEGE and the formulation of the vertical diffusivity scheme in the model. In Section 3, we study changes in the basic physical relationships induced by the resolution refinement. We use data from a turbulence-resolving model, ERA-40 reanalysis and field data from the SHEBA project to assess the differences. We focus on Arctic climate features in Section 4. Section 5 contains a discussion, and conclusions are given in section 6.

2. Turbulence vertical diffusion scheme

Although refinement of the vertical resolution will affect almost all parameterizations in the model, especially the cloud and radiation schemes, we here pay most attention to the turbulence diffusion scheme. In the dry, wintertime Arctic atmosphere, this scheme is the primary agent in forming the temperature profile in the lowest 500 m (Dethloff et al. 2001).

The ARPEGE/IFS model is the atmospheric component of the Bergen Climate Model (Furevik et al. 2003). It was developed by Meteo-France and ECMWF (Deque et al. 1994). The vertical diffusion scheme was developed by Geleyn (1988). It is a first-order eddy-viscosity scheme, which is popular in global models because of its simplicity and physical clarity.

Let ψ be one of the prognostic variables (horizontal components of the wind velocity, moisture or dry static energy). The evolution of ψ due to turbulent transport is given by

$$\frac{\partial \psi}{\partial t} = \frac{1}{\rho} \frac{\partial}{\partial z}\left(\rho K_\psi \frac{\partial \psi}{\partial z}\right) = -g \frac{\partial F_\psi}{\partial p},$$

(2.1)

where ρ is the air density and g is the acceleration due to gravity. A change in the vertical flux with pressure can be regarded as either convergence or divergence of ψ at a given level and thus gives an increase or decrease in the value ψ by time. The vertical flux is given by

$$F_\psi = \rho K_\psi \frac{\partial \psi}{\partial z}$$

(2.2)

The exchange coefficients are either heat, K_h, or momentum, K_m, diffusivities. The exchange coefficient for moisture is assumed to be equal to K_h. They depend on the prognostic variables according to

$$K_m = l_m{}^2 \left|\frac{\partial \vec{U}}{\partial z}\right| \cdot f_m(Ri) \quad \text{and} \quad K_h = \frac{l_m l_h}{l_m{}^2} \frac{f_h(Ri)}{f_m(Ri)} K_m$$

(2.3)

where $f_\psi(Ri)$ is a stability function (Louis 1979) and Ri is the gradient Richardson number. The mixing length scale $l_\psi(z)$ characterizes changes in the turbulent eddy size as a function of the distance from the surface. An empirical polynomial fit is adopted

$$l_\psi(z) = az^3 + bz^2 + \kappa z,$$

$$\begin{cases} a = \dfrac{\kappa H - 2\lambda_\psi}{H^3} \\[2mm] b = \dfrac{3\lambda_\psi - 2\kappa H}{H^2} \end{cases} \qquad (2.4)$$

where H is the boundary layer depth, λ_ψ is the asymptotic length scale, which is generally different for heat (λ_h) and momentum (λ_m), at $z = H$, and $\kappa = 0.4$ is the von Karman constant. The asymptotic length scales for heat and momentum obey the following relation: $\lambda_h = \lambda_m \sqrt{3d/2}$. The stability function is given by

$$f_m^{-1} = 1 + 2bRi(1 + dRi)^{-0.5}, \text{ and}$$

$$f_h^{-1} = 1 + 3bRi(1 + dRi)^{+0.5} \qquad (2.5)$$

where $b=d=5$. It produces a realistic Prandtl-Richardson relation, $\Pr(Ri) = l_m f_m / l_h f_h \gg 1$ for large Ri.

Fluxes at the surface layer are expressed through a bulk approximation

$$F_{\psi s} = \rho C_\psi \|\vec{v}_N\| (\psi_N - \psi_s), \qquad (2.6)$$

where $\|\vec{v}_N\|$ is the wind speed at the lowest model level and $(\psi_N - \psi_s)$ is the difference in ψ between the lowest model level and the surface. The sign of this difference also gives the direction of the flux. The exchange coefficients are

$$C_m = f_m \left(\frac{\kappa}{\ln(1 + z/z_0)} \right)^2 \text{ and } C_h = f_h \frac{\kappa^2}{\ln(1 + z/z_0)\ln(1 + z/z_{0h})}, \qquad (2.7)$$

where z_0 and z_{0h} are the roughness length scales for momentum and heat.

3. Model resolution: coarse versus fine vertical meshes

3.1. Model setup

To study the effect of vertical resolution, we performed a control run of the ARPEGE/IFS with 31 vertical levels in a hybrid sigma coordinate system (Simmons and Burridge 1981), hereafter denoted 31L. The lower levels follow topography, but higher levels become gradually parallel to the pressure surfaces. 8 layers are located below 1600m. The lowest level is at approximately 40 meters height and the next level is close to 140m. The previous discussion indicates that such a standard setup does not resolve the typical Arctic wintertime PBLs. To assure model consistency with differentiation, the minimum H in the 31L configuration is limited to 200 m, equivalent to 2.5 model levels.

To investigate the effect of increased model resolution within the PBL we performed a run with a vertical mesh of 90 levels, hereafter denoted 90L. The resolution was improved only for the lower troposphere below 3000 m. The lowest 5 model levels were located at 10, 20, 30, 40 and 50 meters. Above 50 meters the vertical resolution decreases. In total, 30 layers were added to the lowest 1000 m and 30 layers were added between 1000m and 3000 m. The minimum H was reduced to 20 m, equivalent to 2 model levels. In all other aspects the diffusion scheme was identical to the scheme in the control run. We also performed a 90L simulation with minimum H constrained to 200 m. The results of both 90L runs were very similar. Such a fine vertical resolution in the 90L run should be adequate with regard to most problems related to the coarse mesh representation of strongly curved flux profiles.

The initial and boundary conditions in both experiments were identical and were set up according to AMIP2 requirements and recommendations (AMIP Newsletter, 1996). Both experiments were run with prescribed sea surface temperatures and sea ice for the period January 1979-Decemer 1997 (Smith and Reynolds 2004).

ARPEGE/IFS is a spectral model. Both experiments have the same horizontal resolution defined by a linear triangular truncation at wavenumber 63 (T63). The surface fields have a resolution of 64 latitudes with 128 longitudes around the equator with a reduction poleward.

3.2 Scheme properties on a coarse mesh: a priori test

Observations reveal that the Arctic wintertime PBL is typically very shallow. Figure 1 shows the mean wintertime (DJF) PBL depth from the ERA-40 reanalysis. The mean depth is commonly less than 150 m. This implies that in standard models only 1 to 4 levels are usually located within the PBL. This fact questions the validity of basic assumptions behind the scheme given by Eqs. (2.1)-(2.7). The problems are described in the following paragraphs.

Eq. (2.1) assumes that evolution of the mean quantities can be computed accurately with vertical derivatives of the turbulent fluxes at the coarse mesh resolution. We can estimate the accuracy through a priori testing – a method widely used in computational fluid dynamics (e.g. Brandt, 2006). The method uses exact fluxes or exact profiles of wind speed and temperature as a first-step procedure to analyse the model errors. Firstly we consider errors due to the finite-difference scheme applied to strongly curved flux profiles within the PBL. Analysis of turbulence data and large-eddy simulation modelling (Zilitinkevich and Esau 2005) suggests universal analytical dependencies for momentum and heat for a shear-driven PBL. They are:

$$\frac{F_\psi}{F_{\psi s}} = \exp\!\left(c_\psi \left(z/H\right)^2\right),$$

(2.8)

where c_ψ is a non-dimensional constant, which is -8/3 for momentum and -2 for temperature fluxes, $F_{\psi s}$ is the surface flux, and H is the boundary layer height. Eq. (2.8) can be differentiated both analytically and numerically, and the ratio between the two values gives an estimate of the profile of the error in the term $\partial \psi / \partial t$ due to the implementation of the numerical scheme at the appropriate resolution. Figure 2 shows the tendencies, $H\left(F_{Ts}\right)^{-1}\partial T/\partial t = -\left(F_{Ts}\right)^{-1}\partial F_T/\partial z = -2c_T H^{-2} z\, F_T/F_{Ts}$, for different meshes in the case when the temperature flux is known exactly. In the 31L run with the perfect flux approximation, the differentiation errors lead to considerable additional surface heating as well as a temperature change in the PBL interior which is too weak. The differentiation of the coarsely approximated fluxes thus results in a warm bias in the model. The bias is clearly reduced with the refinement of the vertical resolution as the 90L run shows.

A more rigorous test is based on accurate wind speed and temperature profiles from a high-resolution turbulence resolving model. Figure 3 shows profiles for 31L, 90L approximations and the three-dimensional turbulence-resolving model using a 128^3 mesh with a uniform vertical resolution of 4.7 m (LESNIC, see Appendix for a brief description). In spite of the exact knowledge of the profiles, the gradient Richardson numbers in the approximations differ considerably. The difference results in large errors in H, 248 m in the LESNIC, 500m and 250 m in 31L and 90L runs respectively. Following Troen and Mahrt (1986), the PBL depth, H, is defined as the level where the bulk Richardson number, based on the difference between quantities at a specific level and the lowest surface, reaches the critical value of 0.5. The formulation reads:

$$Ri_j = \frac{(\theta_{vj} - \theta_{v0})g_0 z_j}{\theta_{v0}|\vec{U}_j|^2},$$
(2.9)

Here θ_{vj} is the virtual potential temperature at level j, and θ_{v0} is the virtual potential temperature at the surface, $|\vec{U}_j|$ is the wind speed and z_j is the distance of level j from the surface. g_0 is the acceleration due to gravity.

Figure 4 shows the normalized heat fluxes and the temperature tendencies. The temperature flux in the 31L approximation is about 3 times larger than in the LESNIC and mixes over a much thicker layer. The surface flux, which has been computed from the LESNIC surface temperature, is inconsistent with the flux in the PBL interior. To acheive consistency between the fluxes the surface temperature needs to be increased. This inconsistency could explain a part of the warm bias observed in ARPEGE climatology. It is thus not surprising that the ARCMIP intercomparison experiment (Tjernstrom et al. 2005) indicated no correlation between the observed and modelled surface turbulent fluxes. The thick PBL should also exhibit less temperature variability as it mixes a larger volume of air. This is in line with the weak model variability found in Beesly et al. (2000) in comparison with in situ data from SHEBA. The representation of the heat flux in the 90L approximation is greatly improved in the lowest part of the PBL where the resolution is the finest. The errors in the flux and temperature tendencies increase considerably in the upper part of the PBL where the resolution deteriorates, but the stability increases in the capping inversion. The surface and PBL fluxes are almost consistent in the 90L approximation, suggesting that 10 m vertical

resolution seems to be adequate for the most typical Arctic PBLs. However, inconsistency of the fluxes in the upper PBL will still involve excessive downward heat transport from the free (potentially warmer) atmosphere providing a small warm bias in the 90L experiment. A systematic warm bias in the wintertime GCM simulations was noted by Tao et al. (1996) in most of the AMIP models. It is worth mentioning that enhanced fluxes and a PBL which is too deep are common features of diffusion schemes (Cuxart et al. 2006).

Another way of demonstrating the impact of coarse vertical resolution in to analyse the so-called Smagorinsky-Lilly constant (Lilly 1967), $C_s = l_h \sqrt{f_h(Ri)} / \Delta_z$. The vertical resolution is here described by Δ_z, Ri is the Richardson number, and l_h and f_h are given above. The behaviour of C_s is carefully studied in the laboratory (Liu et al. 1994), the atmosphere (Kleissl et al. 2004) and in many turbulence-resolving simulations (e.g. Mason and Brown 1999; Esau 2004). The constant has been shown to decrease substantially with increasing stability caused either by thermal stratification, the distance from the surface or reduction of the vertical model resolution. The vertical profile of C_s is shown in Figure 5. Unlike other atmospheric turbulence-resolving models (e.g. Beare et al. 2006), LESNIC does not prescribe C_s but computes it dynamically. This feature makes C_s a useful quantity to assess eddy-viscosity turbulence diffusion schemes. In general, the diffusion scheme modifies C_s correctly, reducing it for the coarse resolution meshes. However, the 31L mesh is so coarse that it is not able to produce reasonable profile for C_s. The 90L mesh copes with the task much better, especially when the limit on the minimum mixing length scale is relaxed to $\lambda = 20$ m.

To keep models on track, a number of tuning parameters have been introduced. Parameters from radiation, cloud and turbulence diffusion schemes, such as e.g. λ, interplay making physically correct development of models difficult without a comprehensive retuning. Preliminary intercomparisons with the LESNIC runs suggest an optimal resolution ~10 m for the lower levels in the model. Indeed, the 90L approximation shows significant improvement in representing the turbulent fluxes and tendencies when the limitations on λ have been relaxed.

3.3 Climatology

Figure 6 shows the median PBL depth, H, in the 31L, 90L simulations and the difference between them. When the constraint of 200m is applied on H for the 31L run this shows no similarities with the ERA-40 data. H is for 31L thus computed without applying this constraint. Both the ARPEGE/IFS and the ECMWF (ERA-40) models define H following Troen and Mahrt (1986) (Eq. 2.9). This definition is proved to be reasonable for the PBL developing against the free atmospheric temperature inversion as is the case in the Arctic. Intercomparison between LITE (lidar from space) measurements and ECMWF model results (Randall et al., 1998) suggests that the ERA-40 data overestimate the PBL depth over oceans but give reasonable agreement with the depth over land. The scatter is large, however, since the diagnostic scheme in the model does not account for a number of advection and evolution effects. On basis of this intercomparison, one can expect that the typical PBL depth in the Arctic could be slightly overestimated in ERA-40.

The PBL in the 31L simulation is considerably deeper than in the ERA-40 reanalysis over the Arctic Ocean with a median height north of 80°N of 177m. The 90L run is in this respect a clear improvement, the median PBL height being reduced to141m compared to 136m for the ERA-40 climatology.

Table 1 presents the mean sensible heat flux and net clear sky radiative flux at the surface for the model simulations and for the ERA-40 reanalysis. Beesley et al. (2000) performed comparisons between the ERA-40 reanalysis data and data from the SHEBA project and found that the average surface sensible heat fluxes estimated by the ECMWF model corresponded well with the observations from the SHEBA camp. However, the reanalysis showed large discrepancies on a day to day basis. Curry et al. (2002) also concluded that the ERA-40 surface fluxes agreed well with observations in the Arctic Ocean. During winter over the Arctic Ocean the sensible heat flux is directed from the atmosphere into the surface. This represents heating of the surface and cooling of the near surface air. The 31L simulation underestimates the energy transfer from the atmosphere to the surface compared to the ERA-40 data. The averaged sensible heat flux north of 80°N is in 31L 6.0 Wm^{-2} compared to 11.2 Wm^{-2} in the reanalysis. The sensible heat flux simulated by 90L are in this respect an improvement. The averaged sensible heat flux north of 80°N is 10.6 Wm^{-2} in 90L. Compared to ERA-40 the sensible heat fluxes in 90L becomes too large in the 60-80°N latitude bands.

However, large areas of high baroclinicity are found along the ice edge at these latitudes. These areas represent convective exchange processes that will not be discussed here.

Morcrette (2002) has found the surface clear sky fluxes in the ERA-40 to be reasonable The clear sky fluxes are used instead of the actual fluxes due to considerable biases in the cloud fields in the reanalysis. The model simulations show a generally larger radiative heat loss than the reanalysis. The bias in the 90L simulation is clearly smaller than for 31L. The bias north of 80°N in the 31L simulation compared to ERA-40 is 10.7 Wm^{-2}, this is reduced to 4.8 Wm^{-2} in 90L. The 90L simulation shows a considerable improvement compared to 31L in representing the net clear sky radiative balance north of 60°N as shown in Table 1. The differences in the net surface radiative fluxes are mainly attributed the long wave part since these latitudes receive little or no solar radiation during this season. The change in the net radiation balance is thus directly connected to changes in surface temperature.

3.4 Physical characteristics

To understand changes in the vertical mixing in the ARPEGE/IFS with different vertical resolution, we will compare with in situ data from SHEBA. The Surface Heat Budget of the Arctic Ocean (SHEBA) project (Uttal et al. 2002) collected high vertical resolution data within the PBL during 1997-1998. The observations are taken by a number of instruments at the ice floe camp within the area 70-80ºN and 130-170ºW.

Zilitinkevich and Esau (2003) provided quite robust analytical dependence between the PBL depth and the external governing parameters like the friction velocity, surface sensible heat flux and the free atmosphere stratification. Furthermore, Zilitinkevich and Esau (2005) developed analytical formulations for the resistance laws. The above works demonstrated that properties of the Arctic PBL are different in weak wind and strong wind regimes as well as in weak and strong and atmospheric inversions.

The physical relation between surface winds and surface air temperature is demonstrated in Figure 7. Typically light surface winds corresponds to low surface air temperature (SAT), while stronger winds leads to enhanced vertical mixing and thus higher SAT. For the

comparison of model results with observation and reanalysis data we focus here on three different regimes of surface wind speed.

In the light wind regime with winds in the range 0-6 m/s there is a considerable scatter between the simulations, the reanalysis and observations. Observation data from the SHEBA project reveals that the coldest temperatures are found not under calm wind conditions, but rather for light winds around 3m/s. Data from SHEBA show considerably warmer conditions (approximately 9K) for wind speeds closer to 0m/s. A relation similar to this has also been found by Hudson and Brandt (2005) for temperature inversions on the Antarctic Plateau. The physical explanation for such a relationship relates to advection of cold air from the surrounding continents, which leads to the development of strong inversions together with light winds. When calm conditions occur, however, the convective fluxes of heat from the Arctic Ocean below the sea ice contribute to increase the SAT. The position of the SHEBA camp north of the Alaskan coast should be ideal for such conditions.

This physical relation is not directly captured by the model simulations or the reanalysis. However the temperature sensitivity to wind in ERA-40 is relatively small for winds below 3m/s. SAT in 90L also shows a relatively weak sensitivity to wind speed in this part of the range. It does however not reproduce the low temperatures found for ERA-40. 31L shows a rather opposite relation for light winds, the sensitivity becoming higher for calm winds.

Cases with higher wind speed (in the range 6-12 m/s) show a similar relation between surface winds and SAT for SHEBA, ERA-40 and 90L. Higher wind speeds are typically related to higher SAT. Stronger winds will mix warmer air from higher up in the inversion down to the surface and thus lead to higher SAT. 31L SAT shows a considerably lower sensitivity to changes in surface winds.

For wind speeds above 12 m/s ERA-40 shows generally the same relation between surface winds and SAT as for more moderate wind speeds. 90L and 31L generally predict weaker surface winds than ERA-40, and show considerable scatter in this part of the range. Strong surface winds are related to deeper boundary layers (Eq. 2.9). In these cases the boundary layer will generally be resolved by several model levels also in 31L. The improvement we expect to get by increasing the vertical resolution in the boundary layer will thus be less in

this part of the range. Possible deviations here can be expected to be attributed to other aspects of the parameterization employed in the model.

Figure 8 shows the relation between the vertical gradient in potential temperature in the 925-850 hPa layer ($\nabla\theta$) and SAT. In the simulations and ERA-40 data SAT generally decreases with increasing stratification in the free atmosphere, here represented by the vertical temperature gradient. However the analysis of the data from the SHEBA camp shows a quite different relation, with larger temperature gradient related to higher SAT. The data from SHEBA is quite sparse and shows a relatively large spread. However, data from the LES (not shown) confirms the relation found from SHEBA. The physical mechanism for such a relation can possibly be related to warm temperature advection in the free atmosphere e.g. from synoptic activity. This strengthens the stability calculated as $\nabla\theta$. With the presence of winds the warm air from the inversion layer can be mixed down to the surface layer and thus be related to higher SAT. Such a relation is neither found in the ERA-40 data, nor in the model simulations. SAT in 90L clearly shows a stronger dependence on $\nabla\theta$ than found in 31L and is closer to ERA-40 except for the very low SAT. The distribution of the SAT data in 90L appears more similar to ERA-40. Further studies of this dependency from observations are required to give a robust statement on the quality of this physical relation.

The physical mechanisms which we have described, that govern the vertical exchange processes in stable PBLs, are undoubtedly represented more accurately in 90L than in the 31L simulation. The improved vertical representation is demonstrated in Figure 9. This shows the average vertical profile north of 80°N. Clearly a tropospheric cold bias of -1.5K is evident in the simulations. This can be attributed differences in the large scale circulation patterns in the model and will not be discussed here. The important feature that relates to the vertical exchange processes is the shape of the profile. The improvement in the 90L simulation compared to 31L is evident. Figure 10 shows the dependence of the temperature on key governing parameters in a panel plot for 4 regimes. The regimes are determined as quartiles in the overall wind and stability distribution functions north of 80 degree in 90L, 31L and ERA-40. The 90L simulation shows an overall improvement for all the 4 regimes in comparison with 31L.

4. Interpretation of Arctic Climate features

4.1 Temperature

Liu and Key (2003) found that the temperature inversions in the reanalysis data were too weak compared to the MODIS satellite data. The problem should be largely attributed to the poor vertical resolution in the model. The 90L run shows an increase in static stability. The turbulent mixing is in this case restricted to a considerably shallower layer. This allows formation of radiation inversions in 90L at lower levels. This is a desired modification, which is indicated by observationally based data. The average temperature difference through the inversion layer is increased from 4K to 6K when the vertical resolution is increased in the model.

The surface temperature bias over the Arctic Ocean is reduced in accordance with the reduced vertical mixing in 90L (Figure 11). The general negative biases over high latitude land areas are most likely connected to differences in the lateral energy transports and large scale circulation between the model and reanalysis (e.g. Walsh et al. 2002). For instance the positive trend in the NAO seen in the observations over the analysis period (e.g. Hurrell 1995) is not reproduced in the model simulations. An improved representation of lateral energy transport in the model should rather magnify the positive bias simulated over the Arctic Ocean as a larger amount of heat would be introduced to the Arctic atmosphere. The relation between changes in the boundary layer height and the SAT remain however unclear.

4.2 Moisture response to resolution refinement

In cold wintertime Arctic atmosphere, the maximum long-wave radiation is shifted to the so-called "dirty" window between 18 μm and 25 μm where specific humidity determines opacity of the atmosphere. Thus, the radiative cooling rate becomes sensitive to the accuracy of the temperature simulation in the lower troposphere. Moreover, the relative humidity and thereby cloudiness is sensitive to the inversion temperature as the low-level clouds tend to form within the inversion layer.

In our simulation, the moisture transport and cloud formation schemes have not been changed or tuned to the fine vertical resolution. It allows assessment of the resolution refinement on the moisture and cloud representation in the model.

The inability of the model to properly resolve the temperature profile results in a generally incorrect profile of the relative humidity, R, and thus low-level cloudiness, C_{LL}. Figure 12 shows the vertical profile of relative humidity in the boundary layer from the two simulations and from the vertical soundings from SHEBA. The models generally simulate a moister boundary layer than suggested by the observations. The model PBL has generally highest R near the surface (0-100 m) while in observations R maximizes below the PBL top (100-300 m) in the layer of convergence of downward and upward fluxes. The air above the PBL has a larger absolute humidity but lower R due to higher temperatures in the inversion layer. The 31L run reveals a systematically larger R in the PBL than the 90L run. This feature is in agreement with the effect of reduced vertical turbulent mixing.

5. Discussion

Surface wind speeds are generally too low in the model (31L), the average wind speed being 4.6 m/s in the area north of 70°N compared to ERA-40 data which have an average wind speed of 5.9 m/s. Similar biases are also found at the 850hPa and 700hPa levels. The bias in the wind speed in the control simulation (31L) can be related to biases in the general large scale circulation patterns in the model and will not be discussed in more detail here.

In 90L the surface winds are reduced compared to 31L. This can be related to the stronger stratification in the boundary layer in this simulation. The entrainment of momentum from the free atmosphere down to the surface is reduced. The negative bias in the surface wind speeds increases from 1.3m/s in 31L to 2.2 m/s in 90L. The biases at 850hPa level are -2.4 m/s for 31L and -2.9m/s for 90L. The reduction in the vertical momentum flux is evident. This is in accordance with the Prandtl relation employed in the model parameterisation: a reduction in the vertical momentum flux will follow the reduction in the vertical heat flux. Cuxart et al (2006) evaluated several parameterizations of the stable boundary layer exchange

processes and found that the vertical fluxes of heat and momentum were generally overestimated compared to LES data in most of the parameterizations employed in the large scale climate models. The reduction of the vertical momentum flux in 90L should thus constitute an improved representation of stable boundary layer exchange processes.

The positive surface temperature bias present over the Arctic Ocean in 31L is crucial when introduced to the boundary conditions used in a coupled atmosphere-ocean model system (Curry et al. 2002). The sensitivity of the Arctic climate to a bias in the atmospheric surface flux is high and the biases will typically be enhanced by the positive feedback processes common to the Arctic climate (Colman 2001). The ARPEGE model is employed as the atmosphere component of the Bergen Climate Model (Furevik et al. 2003). Furevik et al. (2003) reported too thin sea ice in the Arctic in the control simulations with the coupled system. The positive temperature bias and the biases in the surface fluxes in 31L constitutes a thermodynamical forcing of the sea ice, and clearly contributes to the thinning of the sea ice (e.g. Bitz and Roe 2004). The improved turbulent exchange processes achieved by improving the vertical resolution in the lower atmosphere reduce the bias in the surface fluxes. This demonstrates the importance of an improved representation of the Arctic atmospheric boundary layer also in coupled atmosphere-ocean models.

Changes in the vertical moisture distribution will clearly affect the frequency of clouds simulated by the model. Comparison of the low cloud cover field from ERA-40 and the simulations reveal that low clouds are more frequent in the reanalysis than in 31L and 90L. Problems with the ERA-40 low cloud cover in the Arctic have been reported by Bromwich et al (2002). Overestimation of the low cloud cover field in ERA-40 is found in comparison with cloud observations from the Environmental Working Group (Arctic Climatology Project 2000). Both model simulations produce less clouds than the ERA-40 over the Arctic Ocean. In the 90L simulation the average total cloud cover is reduced by 5 percent units compared to 31L. The largest reduction in clouds is connected to the low cloud cover field, consistent with the reduction of relative humidity in the boundary layer. The reduction of the low clouds constitutes a small improvement compared to the observation data (Arctic Climatology Project 2000). Average cloud cover in December-February over the Arctic Ocean from the observations is approximately 55%. In the model simulations cloud cover is 70% and 65%, for 31L and 90L respectively. The change in cloud cover characteristics is in accordance with Lane et al. (2000), who found a high sensitivity for cloud cover and related radiative fields

with respect to vertical resolution in a single-column model. By stepwise refinements in the vertical resolution they achieved convergence of cloud frequencies in the model toward the observations. Tao et al (1996) reported that characteristics of clouds in the Arctic as simulated by most GCMs show close to no resemblance with observations. The problems related to the biases in cloud cover in the Arctic are rather connected to inaccuracies in the cloud parameterizations than to the parameterization of vertical exchange processes studied here.

6. Conclusions

Surface-atmosphere exchange in the wintertime Arctic is inhibited by strong stratification in the shallow boundary layers capped by a temperature inversion. This boundary layer cannot be properly resolved by the vertical resolution in the standard version of the ARPEGE/IFS climate model. This is also the situation for the majority of the IPCC climate models. For a coarse vertical mesh (the 31L run with 31 model levels) the vertical diffusion parameterizations are shown to be disadvantageous as their main assumptions cannot be met. To study the effect of the parameterization failure, we performed simulations with a fine mesh. The vertical mesh resolution has been chosen in accordance to the quality criteria based on the LES data.

The fine resolution run 90L has 90 levels with greatly improved vertical resolution close to the surface where the vertical spacing has been reduced to 10 m. The results of the 31L and 90L runs were compared with physical relations derived from in situ (SHEBA) data and with reanalysis (ERA-40) data. The intercomparisons estimate the sensitivity of the model simulations to the vertical resolution in the critical, polar region where climate models demonstrate the largest scatter in future climate projection scenarios.

The sensitivity to the mesh refinement was found to be significant. In the 90L run, the main features of the wintertime Arctic temperature profile – the inversion and cold surface temperatures – were more realistically reproduced. The warm bias in the ARPEGE/IFS model over the Arctic Ocean has been reduced. Surface fluxes and the radiation balance became more realistic. Physical relations that define the surface air temperature were more realistically represented.

The simulated Arctic cloud cover shows considerable sensitivity to the vertical resolution, which is in accordance with the results of Lane et al. (2000). The resolution refinement also caused a number of feedbacks in the model climate. Those feedbacks are beyond the scope of the present study.

Acknowledgements

Appendix

Turbulence-resolving simulations were conducted with the Large-Eddy Simulation Nansen centre Improved Code (LESNIC). The code solves momentum, temperature and continuity equations for incompressible Boussinesq. It employs a number of advanced numerical schemes: a fully conservative 2nd order central difference scheme for the skew-symmetric advection term; the 4th order Runge-Kutta scheme for time stepping; and a direct fractional-step pressure correction scheme for the preservation of continuity. The computational mesh is a staggered C-type mesh, which requires only fluxes as boundary conditions. LESNIC employs dynamic mixed closure, which makes it independent on parameters for manual tuning. The LESNIC computational domain is small, a few kilometres. Along with high mesh resolution it allows for explicit resolution of all energetically important three-dimensional turbulent fluctuations in the planetary boundary layer. The turbulence statistics are then computed from these resolved fluctuations by averaging over the horizontal plane in the domain. A detailed description of the LESNIC was published by Esau (2004), intercomparisons and methods to compute turbulent statistics – in Beare et al. (2006) and Fedorovich et al. (2004).

LESNIC was used in a number of numerical experiments with moderate resolution (64^3), the results from which constitute the DATABASE64. The DATABASE64 was the main source of data for deriving the universal functions in the resistance laws in Zilitinkevich and Esau (2005). LESNIC was also used to compute some runs with much finer resolution as found in the study. All runs were initiated from laminar flow perturbed with energy from computer round-off errors. All runs computed for 16 model hours of which the last hour of data is used to obtain the steady-state turbulent statistics. In all runs the PBL comprises from 1/2 to 2/3 of the total domain depth.

References

AMIP II Guidelines (1996). Program for Climate Model Diagnosis and Intercomparison

Arctic Climatology Project - Environmental Working Group Arctic Meteorology and Climate Atlas. (2000). *F. Fetterer and V. Radionov* National Snow and Ice Data Center. Boulder, CO

ACIA (2004). Arctic Climate Impact Assessment, Cambridge University Press.

Bazile, E., G. Beffrey, M. Joly and H. Marzouki (2005). "Interactive mixing length and modifications of the exchange coefficient for the stable case." Newsletter ALADIN, Météo-France/CNRM/GMAP.

Beare, R. J., I. Esau and etal. (2006). "An intercomparison of large-eddy simulations of the stable boundary layer." Boundary-Layer Meteorology **In press**.

Beesley, J. A. (2000). "Estimating the effect of clouds on the Arctic surface energy budget." Journal of Geophysical Research-Atmospheres **105**(D8): 10103-10117.

Beesley, J. A., C. S. Bretherton, C. Jakob, E. L. Andreas, J. M. Intrieri and T. A. Uttal (2000). "A comparison of cloud and boundary layer variables in the ECMWF forecast model with observations at Surface Heat Budget of the Arctic Ocean (SHEBA) ice camp." Journal of Geophysical Research-Atmospheres **105**(D10): 12337-12349.

Beljaars, A. and P. Viterbo (1999). The role of the boundary layer in a numerical weather prediction model. Clear and Cloudy Boundary Layers. *A. A. M. Holtslag and P. G. Duynkerke*, North Holland Publishers.

Bitz, C. M. and G. H. Roe (2004). "A mechanism for the high rate of sea ice thinning in the Arctic Ocean." Journal of Climate **17**(18): 3623-3632.

Bossuet, C., M. Deque and D. Cariolle (1998). "Impact of a simple parameterization of convective gravity-wave drag in a stratosphere-troposphere general circulation model and its sensitivity to vertical resolution." Annales Geophysicae-Atmospheres Hydrospheres and Space Sciences **16**(2): 238-249.

Boville, B. A. (1991). "Sensitivity of Simulated Climate to Model Resolution." Journal of Climate **4**(5): 469-485.

Bromwich, D. H., S.-H. Wang and A. J. Monaghan (2002). "ERA-40 representation of the arctic atmospheric moisture budget." ERA-40 Report Series **3**: 287-297.

Colman, R. A. (2001). "On the vertical extent of atmospheric feedbacks." Climate Dynamics **17**(5-6): 391-405.

Curry, J. A., J. L. Schramm, A. Alam, R. Reeder, T. E. Arbetter and P. Guest (2002). "Evaluation of data sets used to force sea ice models in the Arctic Ocean." Journal of Geophysical Research-Oceans **107**(C8).

Cuxart, J., A. A. M. Holtslag, R. J. Beare, E. Bazile, A. Beljaars, A. Cheng, et al. (2006). "Single-Column Model Intercomparison for a stably stratified atmospheric Boundary Layer." Boundary-Layer Meteorology.

Deque, M., C. Dreveton, A. Braun and D. Cariolle (1994). "The Arpege/Ifs Atmosphere Model - a Contribution to the French Community Climate Modeling." Climate Dynamics **10**(4-5): 249-266.

Dethloff, K., C. Abegg, A. Rinke, I. Hebestadt and V. F. Romanov (2001). "Sensitivity of Arctic climate simulations to different boundary-layer parameterizations in a regional climate model." Tellus Series a-Dynamic Meteorology and Oceanography **53**(1): 1-26.

Esau, I. (2004). "Simulation of Ekman boundary layers by large eddy model with dynamic mixed subfilter closure." Environmental Fluid Mechanics **4**(3): 273-303.

Fedorovich, E., I. Esau and etal. (2004). Entrainment into sheared convective boundary layers as predicted by different large eddy simulation codes. 16th AMS Symposium on Boundary Layers and Turbulence.

Furevik, T., M. Bentsen, H. Drange, I. K. T. Kindem, N. G. Kvamsto and A. Sorteberg (2003). "Description and evaluation of the bergen climate model: ARPEGE coupled with MICOM." Climate Dynamics **21**(1): 27-51.

Geleyn, J.-F. (1988). "Interpolation of wind, temperature and humidity values from model levels to the height of measurement." Tellus, Series A-Dynamic Meteorology and Oceanography. **40A**: 347-351.

Hogan, T. F. and L. R. Brody (1993). "Sensitivity Studies of the Navy Global Forecast Model Parameterizations and Evaluation of Improvements to Nogaps." Monthly Weather Review **121**(8): 2373-2395.

Hudson, S. R. and R. E. Brandt (2005). "A look at the surface-based temperature inversion on the Antarctic plateau." Journal of Climate **18**(11): 1673-1696.

Hurrell, J. W. (1995). "Decadal Trends in the North-Atlantic Oscillation - Regional Temperatures and Precipitation." Science **269**(5224): 676-679.

Kiehl, J. T. and P. R. Gent (2004). "The Community Climate System Model, version 2." Journal of Climate **17**(19): 3666-3682.

Kleissl, J., M. B. Parlange and C. Meneveau (2004). "Field experimental study of dynamic Smagorinsky models in the atmospheric surface layer." Journal of the Atmospheric Sciences **61**(18): 2296-2307.

Lane, D. E., R. C. J. Somerville and S. F. Iacobellis (2000). "Sensitivity of cloud and radiation parameterizations to changes in vertical resolution." Journal of Climate **13**(5): 915-922.

Lilly, D. K. (1967). "The representation of small-scale turbulence in numerical simulation experiments." Proc. 10th Scientific Computing Symposium on Environmental Sciences, Yorktown Heights, NY, IBM: 195-210.

Liu, S. W., C. Meneveau and J. Katz (1994). "On the Properties of Similarity Subgrid-Scale Models as Deduced from Measurements in a Turbulent Jet." Journal of Fluid Mechanics **275**: 83-119.

Liu, Y. H. and J. R. Key (2003). "Detection and analysis of clear-sky, low-level atmospheric temperature inversions with MODIS." Journal of Atmospheric and Oceanic Technology **20**(12): 1727-1737.

Louis, J. F. (1979). "Parametric Model of Vertical Eddy Fluxes in the Atmosphere." Boundary-Layer Meteorology **17**(2): 187-202.

Mason, P. J. and A. R. Brown (1999). "On subgrid models and filter operations in large eddy simulations." Journal of the Atmospheric Sciences **56**(13): 2101-2114.

Morcrette, J. J. (2002). "The surface downward longwave radiation in the ECMWF forecast system." Journal of Climate **15**(14): 1875-1892.

Overland, J. E. and P. S. Guest (1991). "The Arctic Snow and Air-Temperature Budget over Sea Ice During Winter." Journal of Geophysical Research-Oceans **96**(C3): 4651-4662.

Randall, D., J. Curry, D. Battisti, G. Flato, R. Grumbine, S. Hakkinen, et al. (1998). "Status of and outlook for large-scale modeling of atmosphere-ice-ocean interactions in the Arctic." Bulletin of the American Meteorological Society **79**(2): 197-219.

Randall, D., Q. Shao and M. Branson (1998). Representation of Clear and Coudy Boundary Layers in Climate Models. Clear and Coudy Boundary Layers. *A. A. M. Holtslag and P. G. Duynkerke*. Amsterdam, North Holland Publishers**:** 305-322.

Rinke, A., K. Dethloff, J. J. Cassano, J. H. Christensen, J. A. Curry, P. Du, et al. (2006). "Evaluation of an ensemble of Arctic regional climate models: spatiotemporal fields during the SHEBA year." Climate Dynamics **26**(5): 459-472.

Roeckner, E., R. Brokopf, M. Esch, M. Giorgetta, S. Hagemann, L. Kornblueh, et al. (2006). "Sensitivity of simulated climate to horizontal and vertical resolution in the ECHAM5 atmosphere model." Journal of Climate, in press.

Simmons, A. J. and D. M. Burridge (1981). "An Energy and Angular-Momentum Conserving Vertical Finite-Difference Scheme and Hybrid Vertical-Coordinates." Monthly Weather Review **109**(4): 758-766.

Slingo, A., K. I. Hodges and G. J. Robinson (2004). "Simulation of the diurnal cycle in a climate model and its evaluation using data from Meteosat 7." Quarterly Journal of the Royal Meteorological Society **130**(599): 1449-1467.

Smith, T. M. and R. W. Reynolds (2004). "Improved extended reconstruction of SST (1854-1997)." Journal of Climate **17**(12): 2466-2477.

Tao, X., J. E. Walsh and W. L. Chapman (1996). "An assessment of global climate model simulations of Arctic air temperatures." Journal of Climate **9**(5): 1060-1076.

Tjernstrom, M., M. Zagar and G. Svensson (2004). "Model simulations of the Arctic atmospheric boundary layer from the SHEBA year." Ambio **33**(4-5): 221-227.

Tjernstrom, M., M. Zagar, G. Svensson, J. J. Cassano, S. Pfeifer, A. Rinke, et al. (2005). "Modelling the Arctic boundary layer: An evaluation of six arcmip regional-scale models using data from the Sheba project." Boundary-Layer Meteorology **117**(2): 337-381.

Tompkins, A. M. and K. A. Emanuel (2000). "The vertical resolution sensitivity of simulated equilibrium temperature and water-vapour profiles." Quarterly Journal of the Royal Meteorological Society **126**(565): 1219-1238.

Troen, I. and L. Mahrt (1986). "A Simple-Model of the Atmospheric Boundary-Layer - Sensitivity to Surface Evaporation." Boundary-Layer Meteorology **37**(1-2): 129-148.

Uppala, S. M., P. W. Kallberg, A. J. Simmons, U. Andrae, V. D. Bechtold, M. Fiorino, et al. (2005). "The ERA-40 re-analysis." Quarterly Journal of the Royal Meteorological Society **131**(612): 2961-3012.

Uttal, T., J. A. Curry, M. G. McPhee, D. K. Perovich, R. E. Moritz, J. A. Maslanik, et al. (2002). "Surface heat budget of the Arctic Ocean." Bulletin of the American Meteorological Society **83**(2): 255-+.

Walsh, J. E., V. M. Kattsov, W. L. Chapman, V. Govorkova and T. Pavlova (2002). "Comparison of Arctic climate simulations by uncoupled and coupled global models." Journal of Climate **15**(12): 1429-1446.

Zilitinkevich, S. S. and I. N. Esau (2003). "The effect of baroclinicity on the equilibrium depth of neutral and stable planetary boundary layers." Quarterly Journal of the Royal Meteorological Society **129**(595): 3339-3356.

Zilitinkevich, S. S. and I. N. Esau (2005). "Resistance and heat-transfer laws for stable and neutral planetary boundary layers: Old theory advanced and re-evaluated." Quarterly Journal of the Royal Meteorological Society **131**(609): 1863-1892.

Figure Captions:

Figure 1: *Median PBL height for ERA-40 for December-February 1980-2001. Contours are drawn every 25 m.*

Figure 2. *(a): The exact normalized vertical temperature flux profile approximated with coarse and fine meshes: solid curve – the exact universal profile in Eq. (2.8) derived from the turbulence-resolving simulations; squares – the 31L run approximation of the profile; circles – 90L run approximation of the profile. (b): errors in the normalized temperature tendency induced by second-order differentiation of the exact normalized vertical temperature flux profile from (a).*

Figure 3. *(a) Approximation of exact temperature (solid curve) and wind (dotted curve) profiles taken from a 128 level run of the turbulence-resolving model LESNIC; (b) gradient Richardson number computed from exact and approximated profiles. The solid curves are for the LESNIC, the PBL depth, H = 248 m; squares – the 31L approximation of the profiles; circles – 90L approximation.*

Figure 4. *Computed normalized temperature fluxes (a) and normalized temperature tendencies (b). The solid curves are for the data from the turbulence-resolving model LESNIC where the PBL depth, H , was 248 m; squares – the 31L approximation; circles – 90L approximation. The computation of the surface temperature was parameterized in the LESNIC since model uses the surface fluxes as the boundary conditions. Hence application of the APREGE bulk approximation in the surface layer given by Eqs. (2.6) and (2.7) result in the equal surface heat fluxes in all three models.*

Figure 5. *Computed profiles of the Smagorinsky-Lilly coefficients for vertical diffusion schemes limiting the minimum mixing length scale to 200 m (a) and to 20 m (b). The solid curves are for LESNIC, the PBL depth, H = 248 m; squares – the 31L approximation; circles – 90L approximation.*

Figure 6: *Median PBL height for 31L (upper left), 90L (upper right) and the difference 90L-31L (lower).*

Figure 7: *Relation between surface winds (10m) and surface (2m) air temperature. The upper 4 panels show the density of surface temperature divided in bins of surface winds (grey scatter). This represents the spread around the mean value for each value of surface wind value. The black curve represents the distribution of the wind data. The distribution is for a) ERA-40, b) SHEBA, c) 31L d) 90L. Temperature is on the vertical axis, surface wind speed on the horizontal axis. The lower panel (e) shows the relation between wind and average SAT for ERA-40, SHEBA, 31L and 90L.*

Figure 8: *Relation between surface (2m) air temperature and vertical temperature gradient in the 850-925hPa layer. The upper 4 panels show the density of $\nabla\theta$ divided in bins of SAT. This represents the spread around the mean value for each value of SAT. The black curve*

represents the distribution of the SAT. The distribution is for a) ERA-40, b) SHEBA, c) 31L d) 90L. $\nabla\theta$ is on the vertical axis, SAT on the horizontal axis. The lower panel (e) shows the relation between SAT and average $\nabla\theta$ for the ERA-40, SHEBA, 31L and 90L.
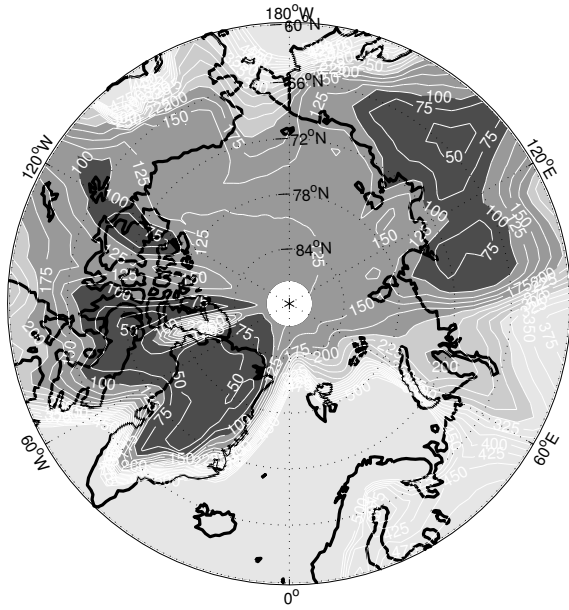
Figure 9: *Average temperature [°C] profile north of 80°N for ERA-40 (solid curve), 31L (dotted curve) and 90L (dashed curve). The horizontal lines denote the 95% confidence interval for the mean value at each level.*

Figure 10: *Same as figure 9, but for 4 different cases separated by upper and lower quartiles key governing parameters. The separation is based on surface wind speed and vertical gradient in potential temperature in the 925-850hPa layer ($\nabla\theta$). Temperature profiles are plotted for a) weak surface winds, b) strong surface winds, c) weak temperature gradient and d) strong temperature gradient.*

Figure 11: *Bias in surface air temperature [K] in 31L (upper left) and 90L (upper right) compared to ERA-40. The difference 90L-31L in lower left. Contours are drawn every 1K. Light shading denotes negative bias, dark shading denotes positive bias.*

Figure 12: *Profile of relative humidity. Vertical axis represents height and is scaled to boundary layer height, H. Units are in percentage.*

Table 1: *Averages of sensible heat flux (SH) and net clear sky radiative heat flux (net R) at the surface for ERA-40, 31L and 90L.*
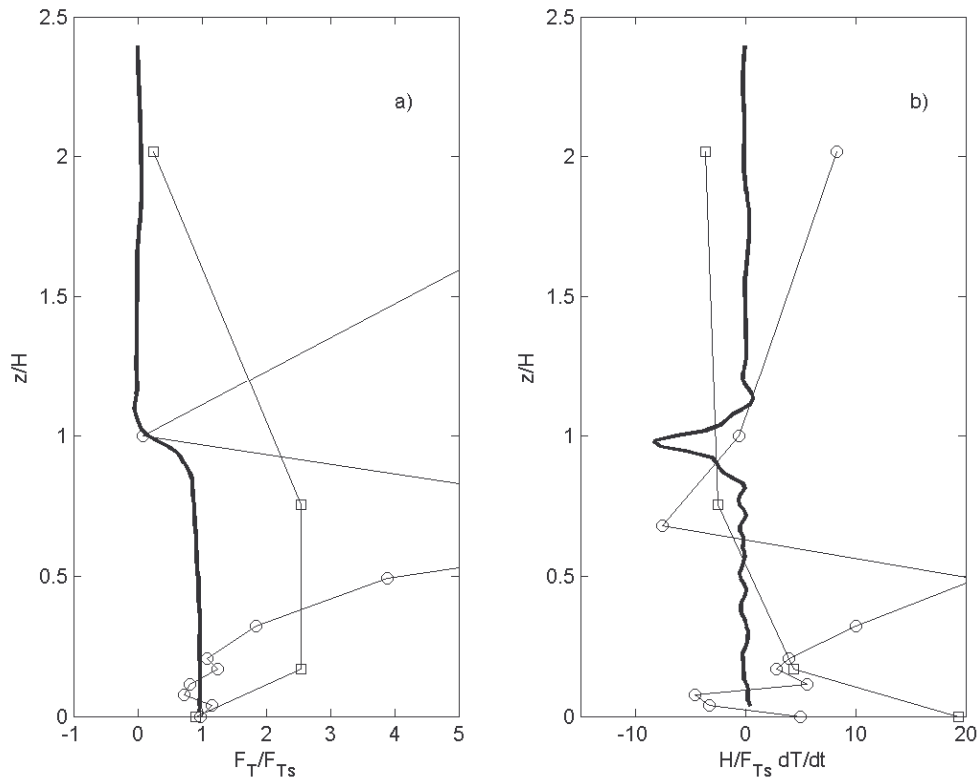
Figure 1: *Median PBL height for ERA-40 for December-February 1980-2001. Contours are drawn every 25 m.*
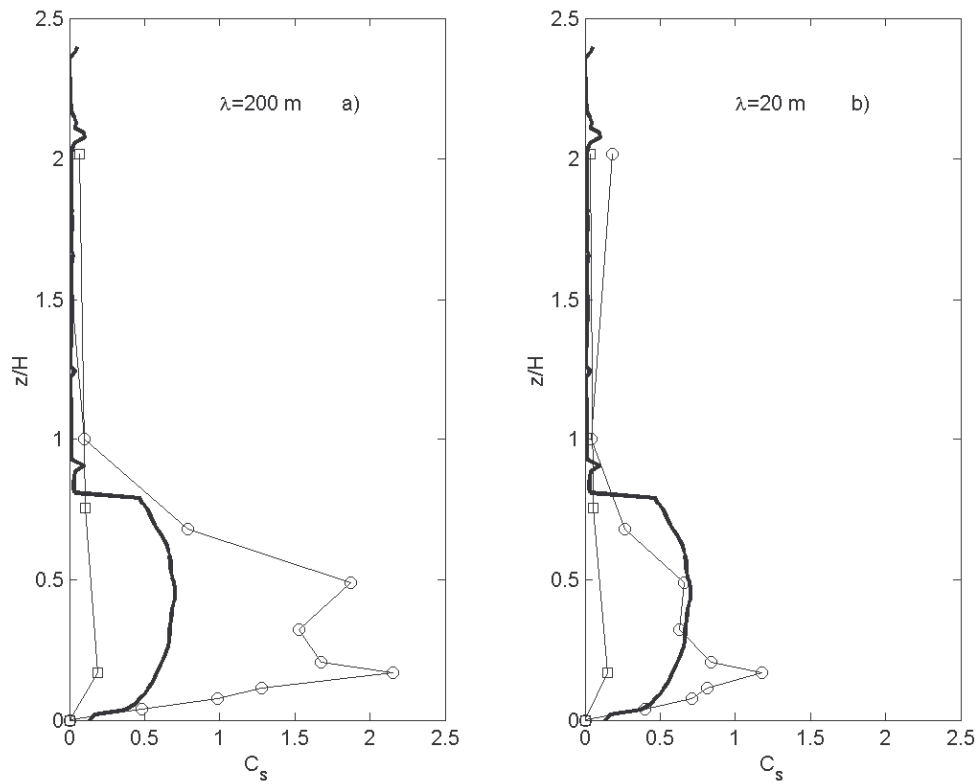
Figure 2. *(a): The exact normalized vertical temperature flux profile approximated with coarse and fine meshes: solid curve – the exact universal profile in Eq. (2.8) derived from the turbulence-resolving simulations; squares – the 31L run approximation of the profile; circles – 90L run approximation of the profile. (b): errors in the normalized temperature tendency induced by second-order differentiation of the exact normalized vertical temperature flux profile from (a).*

Figure 3. *(a) Approximation of exact temperature (solid curve) and wind (dotted curve) profiles taken from a 128 level run of the turbulence-resolving model LESNIC; (b) gradient Richardson number computed from exact and approximated profiles. The solid curves are for the LESNIC, the PBL depth, H = 248 m; squares – the 31L approximation of the profiles; circles – 90L approximation.*

Figure 4. *Computed normalized temperature fluxes (a) and normalized temperature tendencies (b). The solid curves are for the data from the turbulence-resolving model LESNIC where the PBL depth, H, was 248 m; squares – the 31L approximation; circles – 90L approximation. The computation of the surface temperature was parameterized in the LESNIC since model uses the surface fluxes as the boundary conditions. Hence application of the APREGE bulk approximation in the surface layer given by Eqs. (2.6) and (2.7) result in the equal surface heat fluxes in all three models.*

Figure 5. *Computed profiles of the Smagorinsky-Lilly coefficients for vertical diffusion schemes limiting the minimum mixing length scale to 200 m (a) and to 20 m (b). The solid curves are for LESNIC, the PBL depth, H = 248 m; squares – the 31L approximation; circles – 90L approximation.*
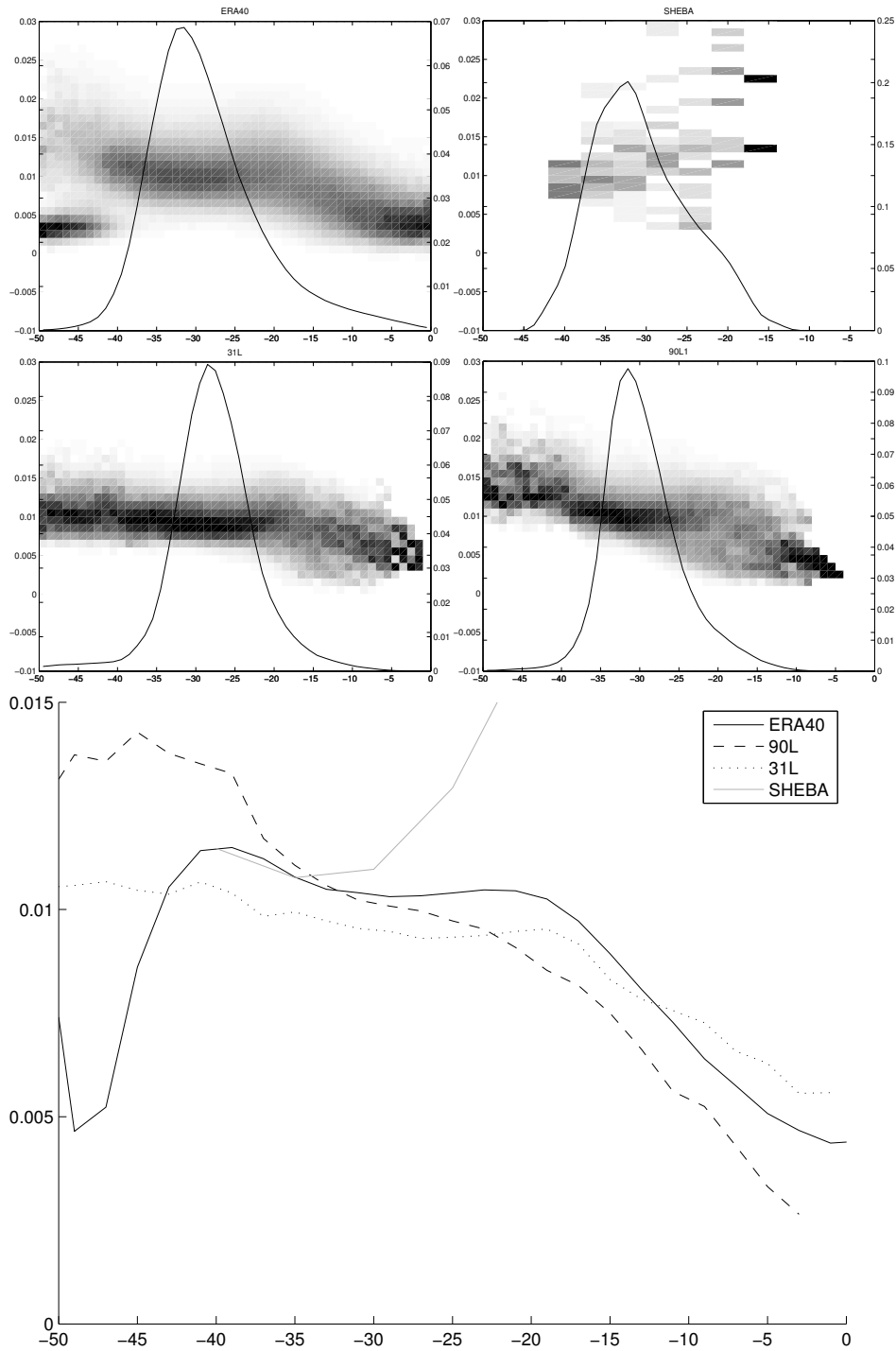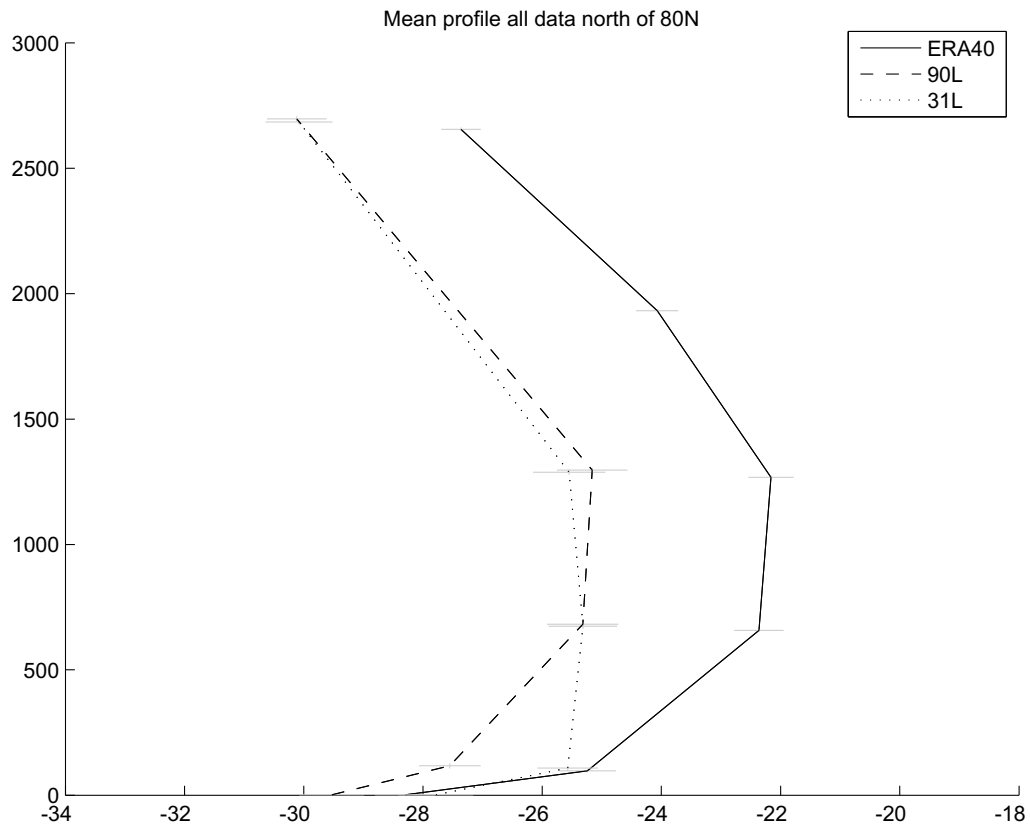
Figure 6: *Median PBL height for 31L (upper left), 90L (upper right) and the difference 90L-31L (lower).*
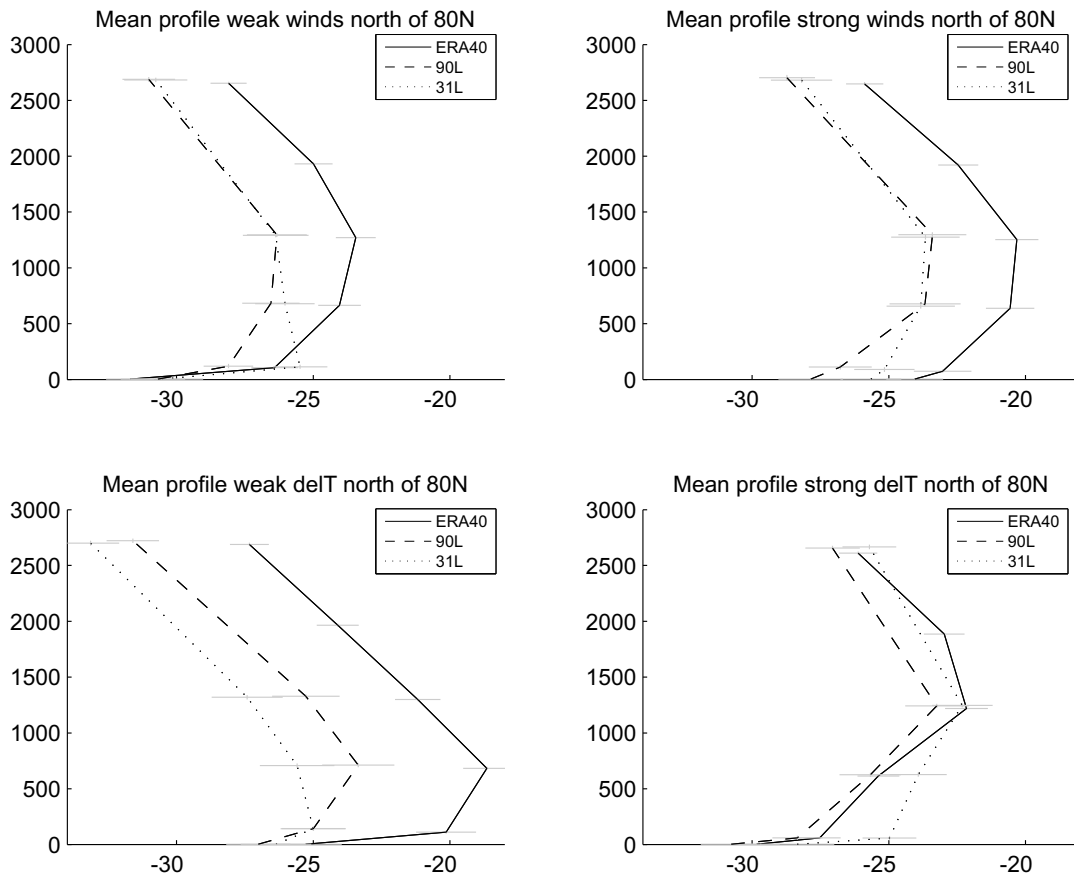
Figure 7: *Relation between surface winds (10m) and surface (2m) air temperature. The upper 4 panels show the density of surface temperature divided in bins of surface winds (grey scatter). This represents the spread around the mean value for each value of surface wind value. The black curve represents the distribution of the wind data. The distribution is for a) ERA-40, b) SHEBA, c) 31L d) 90L. Temperature is on the vertical axis, surface wind speed on the horizontal axis. The lower panel (e) shows the relation between wind and average SAT for ERA-40, SHEBA, 31L and 90L.*
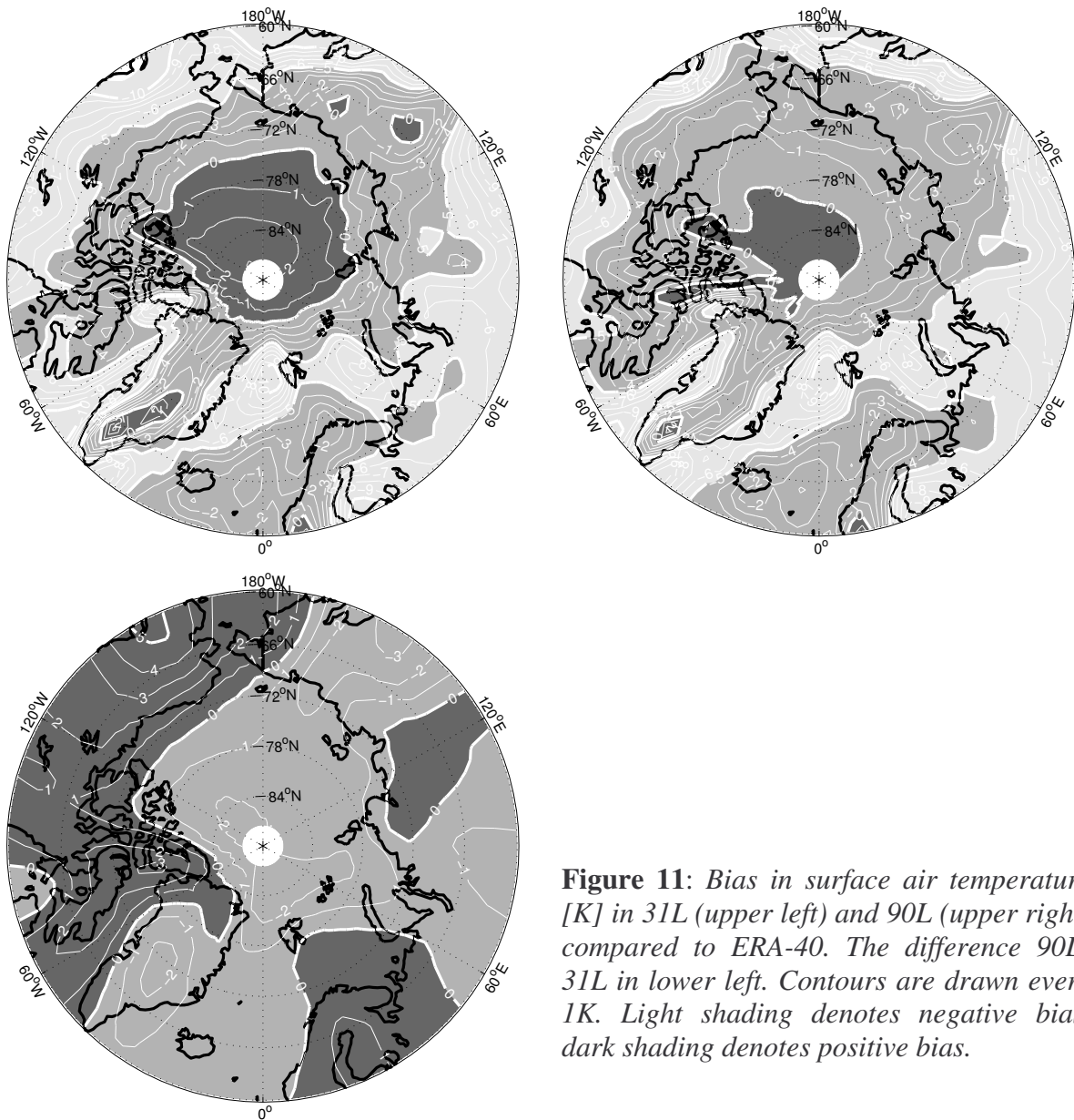
Figure 8: *Relation between surface (2m) air temperature and vertical temperature gradient in the 850-925hPa layer. The upper 4 panels show the density of $\nabla\theta$ divided in bins of SAT. This represents the spread around the mean value for each value of SAT. The black curve represents the distribution of the SAT. The distribution is for a) ERA-40, b) SHEBA, c) 31L d) 90L. $\nabla\theta$ is on the vertical axis, SAT on the horizontal axis. The lower panel (e) shows the relation between SAT and average $\nabla\theta$ for the ERA-40, SHEBA, 31L and 90L.*
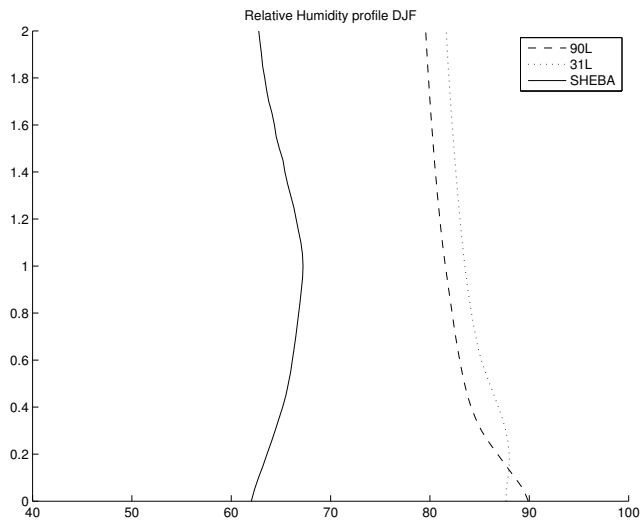
Figure 9: *Average temperature [°C] profile north of 80°N for ERA-40 (solid curve), 31L (dotted curve) and 90L (dashed curve). The horizontal lines denote the 95% confidence interval for the mean value at each level.*

Figure 10: *Same as figure 9, but for 4 different cases separated by upper and lower quartiles key governing parameters. The separation is based on surface wind speed and vertical gradient in potential temperature in the 925-850hPa layer ($\nabla\theta$). Temperature profiles are plotted for a) weak surface winds, b) strong surface winds, c) weak temperature gradient and d) strong temperature gradient.*

Figure 11: *Bias in surface air temperature [K] in 31L (upper left) and 90L (upper right) compared to ERA-40. The difference 90L-31L in lower left. Contours are drawn every 1K. Light shading denotes negative bias, dark shading denotes positive bias.*

Figure 12: *Profile of relative humidity. Vertical axis represents height and is scaled to boundary layer height, H. Units are in percentage.*

	Latitudes	ERA40	31L	90L
SH	80-90°N	11.2 Wm^{-2}	6.0 Wm^{-2}	10.6 Wm^{-2}
	70-90°N	5.3 Wm^{-2}	2.1 Wm^{-2}	7.6 Wm^{-2}
	60-90°N	5.8 Wm^{-2}	1.2 Wm^{-2}	7.4 Wm^{-2}
net R	80-90°N	-64,2 Wm^{-2}	-74,9 Wm^{-2}	-69,0 Wm^{-2}
	70-90°N	-67,3 Wm^{-2}	-74,5 Wm^{-2}	-69,8 Wm^{-2}
	60-90°N	-66,6 Wm^{-2}	-71,5 Wm^{-2}	-67,6 Wm^{-2}

Table 1: *Averages of sensible heat flux (SH) and net clear sky radiative heat flux (net R) at the surface for ERA-40, 31L and 90L.*